https://doi.org/10.17221/178/2020-SWR

Assessment and mapping of soil salinity using electromagnetic induction and Landsat 8 OLI remote sensing data in an irrigated olive orchard under semi-arid conditions

Mohamed Elhedi Gharsallah[1], Hamouda Aichi[2], Talel Stambouli[2], Zouhair Ben Rabah[3], Habib Ben Hassine[2]*

[1]*Laboratory of Agricultural Production Systems and Sustainable Development, National Agronomic Institute of Tunisia, University of Carthage, Tunis, Tunisia*
[2]*Laboratory of Agricultural Production Systems and Sustainable Development, Higher School of Agriculture Education, University of Carthage, Tunis, Tunisia*
[3]*National Center for Mapping and Remote Sensing, Ministry of National Defense, Tunis, Tunisia*

**Corresponding author: hammoud.aichi@ESAMG-u-carthage.tn*

Citation: Gharsallah M.E., Aichi H., Stambouli T., Ben Rabah Z., Ben Hassine H. (2021): Assessment and mapping of soil salinity using electromagnetic induction and Landsat 8 OLI remote sensing data in an irrigated olive orchard under semi-arid conditions. Soil & Water Res.

Abstract: Salinisation threatens the sustainability of irrigated olive orchards in Tunisia. Electromagnetic induction measurements and soil spectral index calculations could help to survey the soil salinity. This study aimed to map changes in the soil salinity spatial pattern using geostatistical techniques and soil spectral index regression. The study area is located in Sminja, Tunisia. It is a 665 ha olive orchard, landscaped in ridges and furrows and managed following a very high-density planting system (1.5 × 4 m^2). Electromagnetic readings measured *in situ* with an electromagnetic device (EM38) that was fitted, in turn, to the electrical conductivity of the saturated paste of five soil depths namely: 0–20, 20–40, 40–60, 60–80 and 80–100 cm and to the average electrical conductivity of the saturated paste of the 0–100 cm soil depth. Both the ordinary kriging and universal kriging performed similarly and well in mapping the soil salinity. (R^2= 0.86 and 0.89 for the 0–20 cm and the 0–100 cm depths, respectively). Our results prove that mapping the soil salinity based on electromagnetic induction and kriging methods is an effective approach, which allows one to monitor the soil salinity within permanent croplands in semi-arid conditions. Salinisation that reaches intolerable values by olive trees, is especially accumulated on the top of the ridges, where the drippers are installed. Furthermore, based on two Landsat 8 images acquired on April 30, 2019 and May 16, 2019, respectively, we calculated seven soil spectral indices. Nevertheless, multiple regression models between the electromagnetic readings and various combinations of soil spectral indices were poor. In the coming investigations, under permanent land cover, spectral index regression models should integrate not only the soil, but also vegetation indices.

Keywords: EM38; geostatiscs; kriging; olive grove; soil salinisation; Tunisia

Over 30% of Tunisian arable land, i.e., 16 800 square km, is devoted to olive growing (Larbi et al. 2016). Tunisia is the fourth largest olive oil producer and the third biggest exporter worldwide (Radinovsky 2019). On the national scale, the olive tree is a strategic crop that plays a crucial socio-economic and environmental role. Indeed, the olive crop represents 15% of the total agricultural production value and

Supported by the National Center of Mapping and Remote sensing (CNCT)-Tunisia and the SPADD Lab, ESA Mograne, University of Carthage. The study was carried out within the context of the soil project of the "Contrat Programme de Recherche" (CPR) of CNCT for data processing and analysis.

https://doi.org/10.17221/178/2020-SWR

its export represents 50% of the total exported agricultural goods (Filippi 2017). In addition, the olive sector offers 34 million working days per year, which represents both the direct and indirect employment of more than 1 million Tunisian people. It also contributes to the preservation of the landscape, and limits the rural exodus. Under a rain fed regime, the olive tree planting density is typically 100 olive trees/ha in the north, compared to 60 and 20 trees/ha in the centre and in the south, respectively (Masmoudi et al. 2017). Whereas, in a conventional irrigated system, typical planting densities are 278 to 330 olives tree/ha. Since the year 2000, an innovative crop system for irrigated olive orchards based on a very high density (VHD) was introduced in Tunisia. Currently, there are 4 500 ha managed according to this crop system in which the inter-rows distance × intra-rows spacing could be 1.5 × 4 m^2 or 1.5 × 3 m^2, which is equal to 1 666 or 2 222 trees/ha, respectively (Larbi et al. 2015). However, in semi-arid and arid conditions, irrigation mismanagement results in soil salinisation issues, which the threatens the crop productivity and sustainability (Hillel & Vlek 2005; Ouji et al. 2015; Boudabous et al. 2016).

In Tunisia, salt-affected soils occupy about 15 000 km^2 which amounts for around 30% of the total arable land of the country (Kahlaoui et al. 2011). Nevertheless, we should differentiate between primary salinity: resulting from natural factors, such as the original salinity of the soil parent material, and climatic aridity, and secondary salinity, also called salinisation: caused by mismanagement of irrigation and drainage practices (Shrestha 2006). Indeed, inadequate irrigation practices can aggravate salinity problems, causing local water tables to rise, which carry the salts to the soil upper layers. This phenomenon endangers the sustainability of cropping systems, through a continuous yield drop and soil degradation (Michot et al. 2013). About 36% of Tunisian irrigated lands are affected by salinisation (Bouksila et al. 2010). Accordingly, surveying the spatial variability of the soil salinity is of great interest in order to carry out or to underpin soil reclamation actions that counteract forthcoming rises in the soil salinity. Most often, assessing and predicting the soil salinity are costly and performed with laborious field sampling (Farifteh et al. 2007; Yao et al. 2008). Therefore, it is of prime importance to explore alternative methods, to investigate the spatial soil salinity. The apparent electrical conductivity (EC) measured by electromagnetic induction (EMI) devices coupled with remote sensing (RS) techniques have been promoted as tools for estimating the soil salinity on different scales (Ding & Yu 2014; Taghizadeh-Mehrjardi et al. 2014; Yao et al. 2015). EMI is a rapid and non-destructive method to measure the EC. Akramkhanov et al. (2014) conducted a repeated EMI survey in Uzbekistan to monitor the soil salinity and considered that the EMI system is an efficient and consistent method. Also, Li et al. (2012) tried to account for the spatio-temporal variations in the total dissolved salts content in arid region of South Xinjiang, China. Furthermore, Liu et al. (2016) have collected EC data with a portable EM38-MK2 device and explored the spatial distribution of the soil salinity in the Yellow River Delta, China, using a geostatistical analysis. In the same framework, Taghizadeh-Mehrjardi et al. (2014) attempted to model the vertical and lateral variation of the soil salinity in central Iran by a combination of an RS and EMI system and, by applying a regression tree analysis, they found that the EC has a significant linear correlation with the electrical conductivity of the soil (ECe) for the upper 0–30 cm layer, whereas a lower correlation was found with the ECe for the bottom 30–60 cm layer. Also, Ding and Yu (2014) combined RS and EMI in order to screen and evaluate the spatial and seasonal changes of the soil salinity, and they proved that the spatial distribution of the soil salinity differed from small vertical or horizontal distances and that dissolved salts remain concentrated in the surface which limits their mobility in arid and semi-arid areas. By combining RS and EMI techniques, Wu et al. (2009) studied the spatial variation of the soil salinity in Feng-qiu County, China, and established regression models between the field measured EC and the soil and vegetation spectral indices. Therefore, compared to conventional field work and the ensuing laboratory measurements, the combination of EMI and remote sensing data can be useful to predict the ECe fairly, rapidly and accurately (Liu et al. 2003; Zhang et al. 2009). Kriging techniques, such as ordinary kriging (OK), universal kriging (UK), indicator kriging and co-kriging, refer to a group of geostatistical interpolation methods. Kriging is the most appropriate to interpolate soil data, for which there is a spatially correlated distance or directional bias. It assumes that the distance or direction between the sample points reflects a spatial correlation that can be used to explain the variation in the surface (Knotters et al. 2010). Kriging serves to predict the value at one unobserved point based on a linear combination of the values at neighbouring

https://doi.org/10.17221/178/2020-SWR

observed points, the weights for the observed points are attributed according to a model that describes the spatial structure of the environmental variable (Webster & Oliver 2007). The most general and widely used kriging method is OK. However, the choice of which kriging method to use depends on the spatial structure of the environmental variable. For instance, in a case where the distribution of the environmental variable shows a strong trend, UK, also referred to as kriging with a trend model, may perform better than OK (Mesić Kiš 2016). Kriging is performed in two-steps. In the first step, an empirical semi-variogram is computed for all pairs of locations separated by distance h. The semi-variogram can be defined as the average squared difference between the components of the data pairs (Oliver & Webster 2014) as in the following equation:

$$\gamma(h) = \frac{1}{2N(h)} \sum_{i}^{j} \in N(h) \left(z_i - z_j\right)^2 \quad (1)$$

where:

$N(h)$ – the number of pairs of observations (i, j) separated by a spatial distance h;

z_i, z_j – the attribute values of the i and j observations, respectively.

In the second step, a model is fitted to the cloud of points forming the empirical semi-variogram, and then it is used for the prediction in unsampled locations. Kriging forms weights from the surrounding measured values to predict the unmeasured locations. The empirical semi-variogram graph, depicts the spatial dependence in the attribute values of the observations. Three characteristics serve to describe the fitted model: (*i*) the range is the spatial distance from which the observations are no longer auto-correlated, where the model first flattens out. (*ii*) the sill, corresponds to the value on the y-axis, at which the semi-variogram model attains the range, and (*iii*) the nugget corresponds to the model semi-variogram value at zero separation distance. The nugget effect represents small-scale spatial variations. This parameter indicates how noisy the spatial structure is (Figure 1).

The objectives of this study were to (*i*) investigate the spatial and the depth of the soil salinity changes on the local-scale of the RF landform, (*ii*) predict the ECe at various soil depths based on the EM 38 readings, (*ii*) map the ECe in the study zone for the soil depths demonstrating the highest correlations between the ECe measured in the laboratory and predicted based on the EM38 readings, (*iii*) attempt to calibrate the spectral models of the pedo-transfer that match the predicted ECe values with several derived soil spectral indices.

MATERIAL AND METHODS

Study area. The study area is situated between 9°59'8''E~10°1'37''E longitude and 36°26'30''N~36°28'30''N latitude. It lies in the south of the Bir Mcherga Dam, in the north-west of the governorate of Zaghouan, 50 km south from the capital Tunis (Figure 2). The land area covers 6.65 km^2 and belongs to an agribusiness firm. As a part of the Sminja plain, the landform of the study area is almost flat. The elevation ranges between 141 m a.s.l. in the south end, and 117 m a.s.l. in the north end, with a gentle, but regular, slope of 0.96% in a south-west/north-east direction, oriented from the plain to the riparian dam. The study area is characterised by a semi-arid climate. The average annual rainfall recorded over the last 11-years is 390 mm. The rainfall is concentrated in the autumn and winter accumulating 75% of the total annual precipitation on average. Whereas the spring and the summer are dry seasons accumulating 21 and 4% of the average total annual precipitation, respectively. A large water deficit occurs during these two dry seasons. The monthly average temperature ranges between 8 °C in January and 42 °C in August with an annual average of 18 °C. The soils of the study area are composed of deep monolithic Vertisols. They are

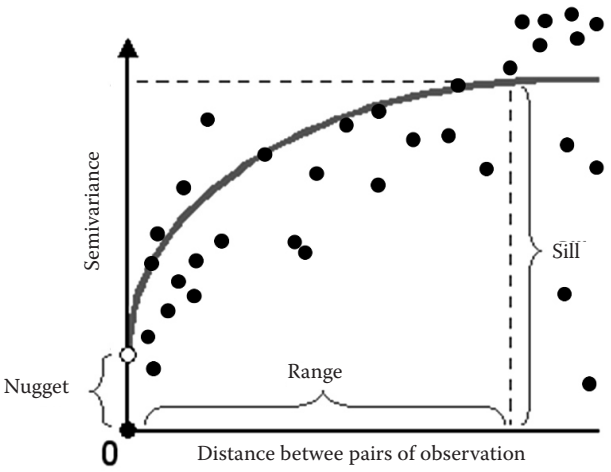

Figure 1. Illustration of the empirical semi-variogram (cloud of points), fitted by an exponential function and model range, sill, and nugget components (Oliver & Webster 2014)

https://doi.org/10.17221/178/2020-SWR

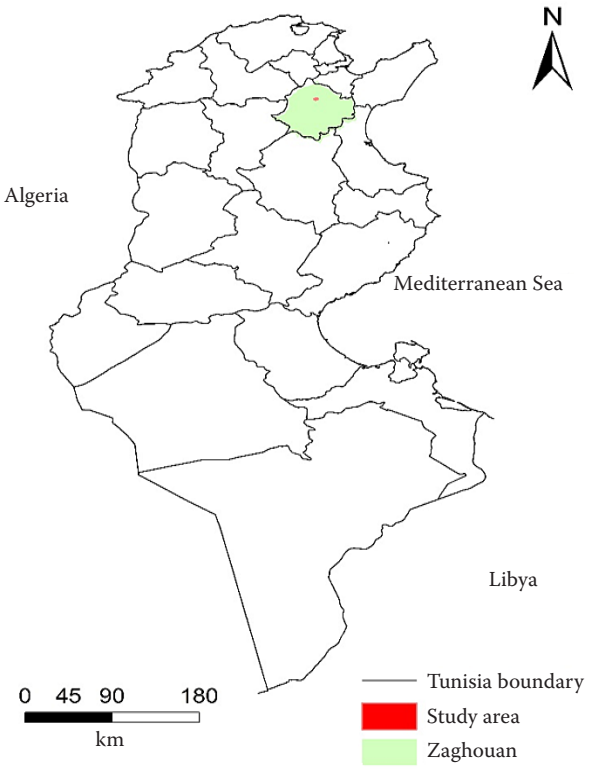

Figure 2. Location of the study area on the administrative map of Tunisia

the product of the weathering of marl rock. These soils are characterised by a high swelling clay content, a high limestone content, an alkaline pH, a clay loamy texture, and a low hydraulic conductivity in a saturated condition. The surface horizon and the bottom horizon have granular and block-like structures, respectively. These soils are be suitable for other fruit tree crops. The land cover of the study area is an evergreen olive orchard managed following a crop mix system, made up of two introduced varieties, namely: Arbosana and Arbequina. This olive orchard was created twenty-two years ago in 1999, according to a VHD pattern. Indeed, the planting density is 4 × 1.5 m^2 and the trees are cultivated in hedges, with an annual average yield of 7–8 t/ha. The land surface is landscaped using a ridge and furrow RF planting pattern, which consists of shaping ridges and alternating then with furrows. The trees are planted into the top of the ridges which are raised 1 m above the level of the furrows. The RF system enables one to capture the rainfall well, to improve the water-use efficiency and to mitigate the harmful effects of the accumulation of salts within the root zone, especially because the soil poorly drains and is an asphyxiant (Masmoudi et al. 2017) (Figure 3). The olive orchard is supplied with water from the Bir Mcherga Dam. The motor-pump units installed at the edge of the dam's reservoir deliver the water into a geo-membrane collection basin with a capacity of 5 000 m^3. After filtration, this water is distributed into the drip irrigation network. The olive orchard is particularly irrigated in the spring and the summer dry periods. The salinity of the dam water varies on an annual and inter annual scale, according to the rainfall. Over the last ten years, the annual average salinity was 2.6 g/L. Nevertheless, in May 2019, the dam water salinity was equal to 5.8 g/L and the electrical conductivity was equal to 7.6 dS/m. The water supply is modulated according to the amount of rain that has fallen, which is especially provided during the spring and summer dry seasons.

Field campaign. The field campaign, including the soil sampling and EM38 readings, occurred from 1 to 16 May, 2019. This matches the start of the dry season, during this period, the soil, not yet irrigated, is at its maximum dryness. Indeed, water is only supplied during the dry season.

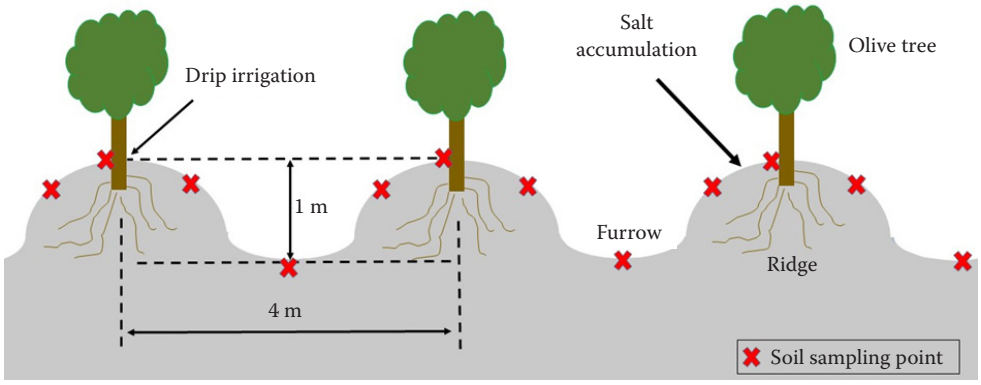

Figure 3. Cross-section of three planted ridges within the study area

https://doi.org/10.17221/178/2020-SWR

Changes in the salinity of the soil profile, between the ridges and furrows. In the preliminary stage, we investigated the changes in the salinity of the soil profile between the ridges and furrows and described how the accumulation of salt in the soil profile could vary over short distances depending on the cropland micro-relief. Thus, two transects of 9 linear meters each alongside two olive orchard diagonals were prospected. The samples were collected into the three micro-morphologies of the cropland namely: furrows, flanks, and peaks of the ridges. Twenty-four surveyed locations were sampled (4 ridges + 4 flanks + 4 furrows) × 2 transects). To have a continuous characterisation of the soil salinity profile, at each prospected location, the soil was sampled using a manual auger (diameter = 7 cm) at five depths (0–20, 20–40, 40–60, 60–80 and 80–100 cm). A total of 120 soil samples were collected within the study area (24 prospected locations × 5 depths). This first set of samples was brought to the laboratory, air-dried, crushed and sieved through a 2 mm sieve then analysed for the ECe according to the standard method (Richards 1954).

EM38 calibration. The calibration of the EM38 device (Geonics, Ltd., Mississauga, Canada), consists of converting the readings acquired in the vertical mode (EC_V) and in the horizontal mode (EC_H) in the field into ECe, (Amezketa 2007). In our case, ten geo-referenced RF micro-relief locations, evenly spread across the entire study area were selected. For each location, two points, spaced by 2 m from each other, the first into the ridge and the second into the neighbouring furrow, were surveyed. For each point, a pair of EM readings were made, the first one with the coil of the EM38 device positioned horizontally to the soil surface for the EC_H and the second one with the device positioned vertically for the EC_V. After each pair of EM38 readings, the soil sampling was systematically carried out for every 20 cm of depth up to 100 cm. That is, at five depths, namely: 0–20, 20–40, 40–60, 60–80 and 80–100 cm. Thus, a total of 100 samples were collected (10 (survey sites) × 2 (a couple of points, one in the ridge and a second in the furrow) × 5 (depths)) (Figure 4). This second set of soil samples was brought to the laboratory, air-dried, crushed and sieved through 2 mm sieve and then analysed for the ECe as well.

Thereafter, six separate calibration equations were established to investigate the relationship between the ECe at various depth and the EM38 readings. The first five Equations correspond to the five successive soil depths, respectively, and the sixth equation corresponds to the average ECe referred to as $ECe_{(0–100\ cm)}$. $ECe_{(0–100\ cm)}$, was calculated according to the following formula:

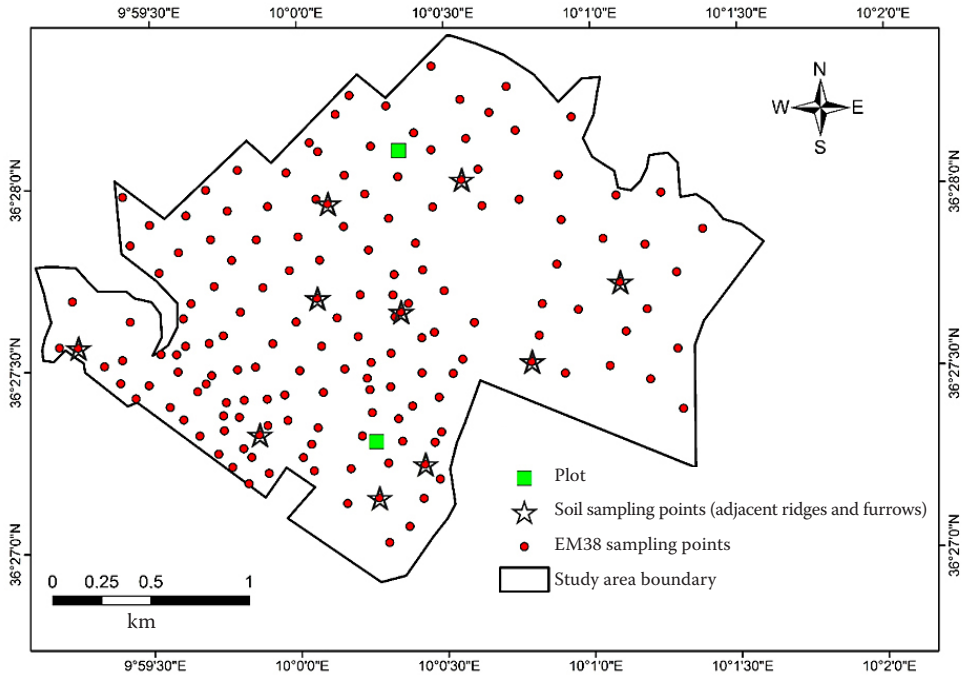

Figure 4. Location of the study area, ground sampling points and EM38 measuring sites; the plots refer to the small locations where the transects were prospected

https://doi.org/10.17221/178/2020-SWR

$$ECe_{(0-100\ cm)} = [2ECe_{(0-20\ cm)} + 1.5ECe_{(20-40\ cm)} + + ECe_{(40-60\ cm)} + 0.5ECe_{(60-80\ cm)} + + 0.25ECe_{(80-100\ cm)}]/5 \quad (2)$$

The weighting factor, attributed to the ECe of each depth, is proportional to the fraction of the roots which colonise that depth. That is, proportional to the contribution of each depth to the water uptake by the olive tree (CRUESI 1970; Hachicha 2016).

ECe prediction and spatial interpolation. The EM readings data that served to first predict then to interpolate the ECe by kriging methods were collected in 160 RF locations adequately covering the whole study area. In each location, the EM readings (EC_H and EC_V) were carried out in two close points, spaced by 2 m, the first into the ridge and the second in the closest neighbouring furrow. In each point, the reading was successively made in the horizontal and then in the vertical mode. In total, 640 EM readings were taken (160 (locations) × 2 (RF) × 2 (pairs of reading in the vertical and horizontal modes)). The locations were georeferenced by GPS (Trimble® GeoExplorer XM series 3000) with a precision of 1–3 m. (Figure 4). The ECe predictions on the 160 EM reading served to spatially interpolate the ECe in the study area. Using the geostatistical analyst tool implemented in ArcGIS® 9.3.1, two geostatistical methods were used and compared to assess which one performed better, namely: OK as it is the default method, but also the UK method since, in our study area, a gentle, but regular, slope prevails, which could hide an overriding trend in the spatial structure of the variable. The two methods were compared for their effectiveness. The accuracy of the produced maps were assessed using the leave one-out cross validation. Three criteria were calculated to evaluate the performance of the regression models, namely, the mean error (ME), root mean squared error (RMSE), and coefficient of determination (R^2). The formulas of these criteria are as follows:

$$ME = \frac{\sum_{i=1}^{M}\left[Z^*(Si) - Z(Si)\right]}{M} \quad (3)$$

$$RMSE = \sqrt{\frac{\sum_{i=1}^{M}\left[Z^*(Si) - Z(Si)\right]^2}{M}} \quad (4)$$

$$R^2 = \frac{\sum_{i=1}^{M}\left[Z^*(Si) - Z(Si)\text{ave}\right]^2}{\sum_{i=1}^{M}\left[Z(Si) - Z(Si)\text{ave}\right]^2} \quad (5)$$

where:

$Z^*(Si)$ – the interpolated value;

$Z(Si)$ – the observed value;

$Z(Si)$ ave – the average of the observed values;

M – the number of samples (160).

The ME measures how far away the errors are from the actual value. The smaller RMSE indicates a better fit.

Remote sensed data and derived spectral salinity indices. The images used in this study were obtained from the Landsat 8 Operational Land Imager (OLI-8). They were acquired on April 30, 2019 and May 16, 2019. These dates match with the period of the field campaign. These images were at the end of spring and the beginning of summer. During this period, the irrigation had not yet started in the olive orchard, and the salts accumulated in the soil profile are at their highest concentrations. Indeed, one of the adopted practices, particularly during the summer, to manage the salinity, consists of draining the salts out of the root zone, by majoring the water requirements with a leaching fraction.

Atmospheric and radiometric corrections were implemented for each band separately. The COST model (the COSine of sun zenith angle (T)) by Chavez (1996) was used to convert digital numbers to surface reflectance for both images by using the Environmental for Visualizing Images (ENVI Ver. 5.2) software package®.

We calculated seven relevant and well-known, in the literature, soil salinity spectral indices. They are as follows: the normalised difference vegetation index (NDVI) (Deering & Rouse 1975), the difference vegetation index (DVI) (Tucker 1979), the brightness index (BI) (Khan et al. 2005), the salinity ratio (SR) (Metternicht & Zinck 2003), salinity index 1 (SI1) (Douaoui et al. 2006), salinity index 2 (SI2) (Bannari et al. 2008), and salinity index 3 (SI3) (Abbas & Khan 2007). The calculation formulas for these indices are summarised in Table 1.

Once the matrices of these indices were calculated using the spatial analyst tool (Extract Multi Values to Points) implemented in the ArcGIS® Ver. 9.3.1 software, we simultaneously extracted, from these matrices, the pixel values that match the 320 EM38's field readings. While exploring various combinations of these soil salinity indices as dependent variables and the predicted ECe (based on EM38 measurements) as the independent variable, we established several multiple linear regressions and assessed their

https://doi.org/10.17221/178/2020-SWR

Table 1. Soil salinity indices based on the different band ratios of the Landsat 8 OLI

Spectral index	Calculation formula	Reference
Normalised difference vegetation index (NDVI)	$NDVI = \frac{\rho OLI5 - \rho OLI4}{\rho OLI5 + \rho OLI4}$	Deering and Rouse (1975)
Difference vegetation index (DVI)	$DVI = \rho OLI5 - \rho OLI4$	Tucker (1979)
Brightness index (BI)	$BI = \sqrt{(R^2 + NIR^2)}$	Khan et al. (2005)
Salinity ratio (SR)	$SR = \frac{\rho OLI4 - \rho OLI5}{\rho OLI3 + \rho OLI5}$	Metternicht and Zinck (2003)
Salinity index 1 (SI1)	$SI1 = \sqrt{(\rho OLI3^2 + \rho OLI4^2 + \rho OLI5^2)}$	Douaoui et al. (2006)
Salinity index 2 (SI2)	$SI2 = \frac{\rho OLI3 \times \rho OLI4}{\rho OLI2}$	Bannari et al. (2008)
Salinity index 3 (SI3)	$SI3 = \frac{\rho OLI5 \times \rho OLI4}{\rho OLI3}$	Abbas and Khan (2007)

prediction performances. If the assessment of these models linking the predicted ECe (based on EM38 readings) to the combination of the spectral indices prove that they perform well, then they could serve, in the future, at least to monitor changes in the spatio-temporal soil salinity, with no need for soil sampling and ECe analysis in the laboratory. The calibrated models were assessed by calculating the ME, the R^2 and the RMSE, between measured and predicted values, as well.

RESULTS AND DISCUSSION

Changes in the salinity of the soil profile between the ridges and furrows. In the two investigated transects, the laboratory analysis revealed that the salt distribution in this irrigated area displays an abrupt change between the ridge and the furrow. Such a result is essentially due to the irrigation system (drip) and the surface geometry (Figures 5A, B). However, salts mostly accumulated in the side and the top of the ridges in contrast with the furrows. The ridges are separated by the furrows 4 m in width as well. Many geostatistical studies of soil salinity data (Douaoui et al. 2006; Michot et al. 2013) have underlined the variability in the soil salinity over short distances. Consequently, we have developed two distinct maps, one for the spatial distribution of the soil salinity in ridges and the other for the spatial distribution of the soil salinity in furrows.

Descriptive statistics of the EM38 readings and the ECe. The summary statistics of the soil EM38 readings and the ECe at the five sampled depths (0–20, 20–40, 40–60, 60–80 and 80–100 cm) are displayed in Table 2. The mean ECe for the five sampled depths ranged between 5.62 and 8.27 dS/m in the soil profiles. ECe (0–20 cm) was the highest, which indicates that salts have accumulated in the surface layer, especially in the top layer, where the ECe varied from 0.47 to 26.1 dS/m. The coefficient of variation of the ECe for the five sample depths ranged from 0.61 to 0.96 displaying strong spatial variability. Moreover, the EC values measured under the horizontal and vertical modes ranged between 32 and 278 mS/m.

Prediction of ECe based on EM38 readings. First of all, we used linear regression analysis between the ECe values of each layer and the EC measurements taking the EM38 readings (EC_H and EC_V) as independent variables. The results showed that multivariate models give the best fit (R^2 between 0.63 and 0.89), which are presented in Table 3. Compared to the simple regression on the EC_H or on EC_V each taken separately, the results are not shown here.

In addition, the scatter plots of the measured vs. predicted for each depth and the average the ECe are shown in Figure 6. Scatter plots of: (A) 0–20 cm, (B) >20–40 cm, (C) >40–60 cm, (D) >60–80, (E) >80 to 100 cm and (F) 0–100 cm using calibrated models.

From this figure, we remarked that the predicted ECe of the top two depths and the average ECe had better accuracies, while the remaining depths were less accurate.

Spatial interpolation using OK and UK. For both the OK and UK methods, the 160 ECe values derived

https://doi.org/10.17221/178/2020-SWR

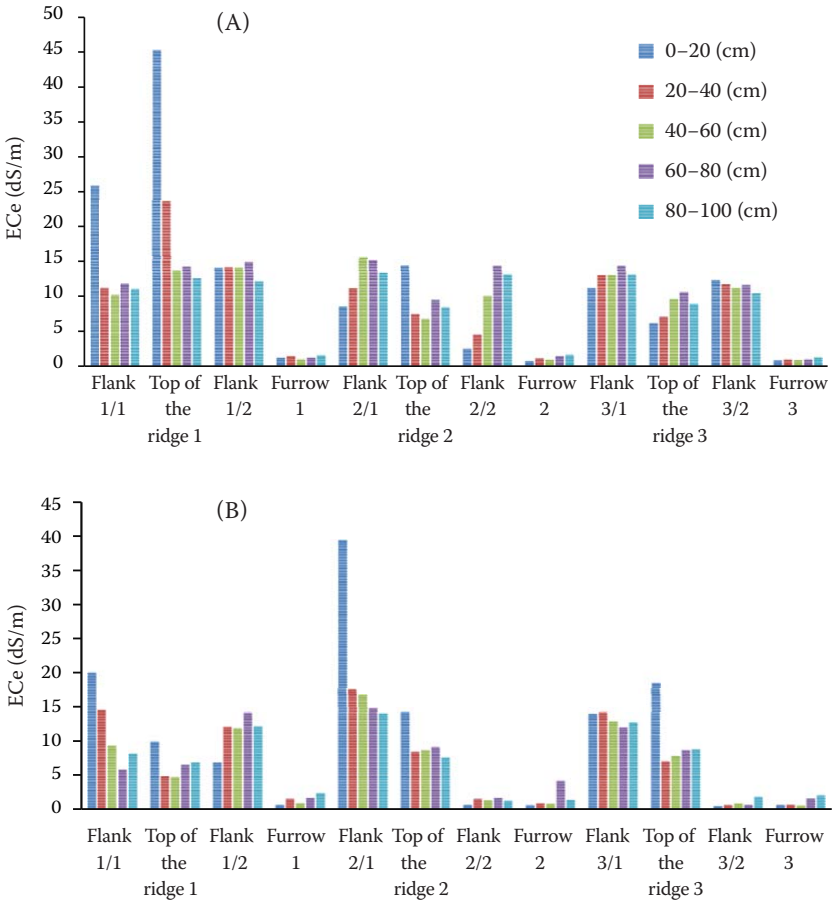

Figure 5. Distribution of the soil electrical conductivity (ECe) in two distinct transects made up of three consecutives ridges and furrows: southern plot (A), northern plot (B)

from the EM38 measurements (EC_H and EC_V) were fitted with an exponential theoretical model using the geostatistical analyst tools in ArcGIS® Ver. 9.3.1 (Table 4). The ECe variable is considered to be anisotropic, i.e., there is a directional effect and the variable does not vary in the same way in all directions, to find the best theoretical description of the spatial structure characteristic in the ECe in the study area. The cross-validation test indicates that the exponential model gives the best fit (the R^2 between the observed and fitted values is 0.79 and 0.92 for the furrows and for the ridges, respectively) for both the OK and the UK (Table 5). The maps of the ECe (0–20 cm) and average ECe (0–100 cm) for both the ridges and the

Table 2. Descriptive statistics of the soil ECe and electromagnetic readings

Layer (cm)	N	Min	Max	Average	SD	*CV*	Skewness
ECe (0–20)	20	0.47	26.1	8.27	7.9576	0.9618	0.6067
ECe (> 20–40)	20	0.53	13.2	5.62	4.5088	0.8018	0.2175
ECe (> 40–60)	20	0.64	14.08	5.93	4.7273	0.7976	0.2377
ECe (> 60–80)	20	0.82	12.74	6.11	4.4197	0.7236	0.0168
ECe (> 80–100)	20	0.93	12.04	6.5	4.0183	0.6179	–0.1771
Average ECe	20	0.61	19.24	7.09	6.00	0.8470	0.3701
EC_V ridge	1.60	0.43	2.14	0.81	0.26	0.03	6.44
EC_H ridge	1.60	0.49	2.08	1.37	0.28	0.21	–0.02
EC_V furrow	1.60	0.69	2.78	1.26	0.39	0.31	2.84
EC_H furrow	1.60	0.32	2.41	0.64	0.34	0.53	11.93

ECe – soil electrical conductivity (dS/m); EC_V – electrical conductivity, device positioned vertically (dS/m); EC_H – electrical conductivity, device positioned horizontally (dS/m); SD – standard deviation; *CV* – coefficient of variation

https://doi.org/10.17221/178/2020-SWR

Table 3. Soil electrical conductivity (ECe) prediction t models for the different soil depths based on the electromagnetic readings under the horizontal and vertical modes, as independent variables

Soil layer (cm)	ECe= $a + bEC_H + cEC_V$			
	a	*b*	*c*	R^2
0–20	2.98993	0.13400	–0.08065	0.86
> 20–40	1.97311	0.07826	–0.04176	0.87
> 40–60	1.29518	0.08076	–0.03492	0.79
> 60–80	1.11311	0.07629	–0.02712	0.78
> 80–100	2.82511	0.06158	–0.02524	0.63
Average ECe	2.42436	0.10478	–0.05804	0.89

furrows were produced using OK which was the same as the UK (the same R^2). These maps are displayed as Figure 6A, B and Figure 7A, B, respectively. From the figures, it is easy to realise that the extremely salinised part (high level of ECe derived from the EM38 readings) represents almost all the irrigated area, except for the southern border (for the ridges) and a small, salinised region in the north-west of the olive orchard (for the

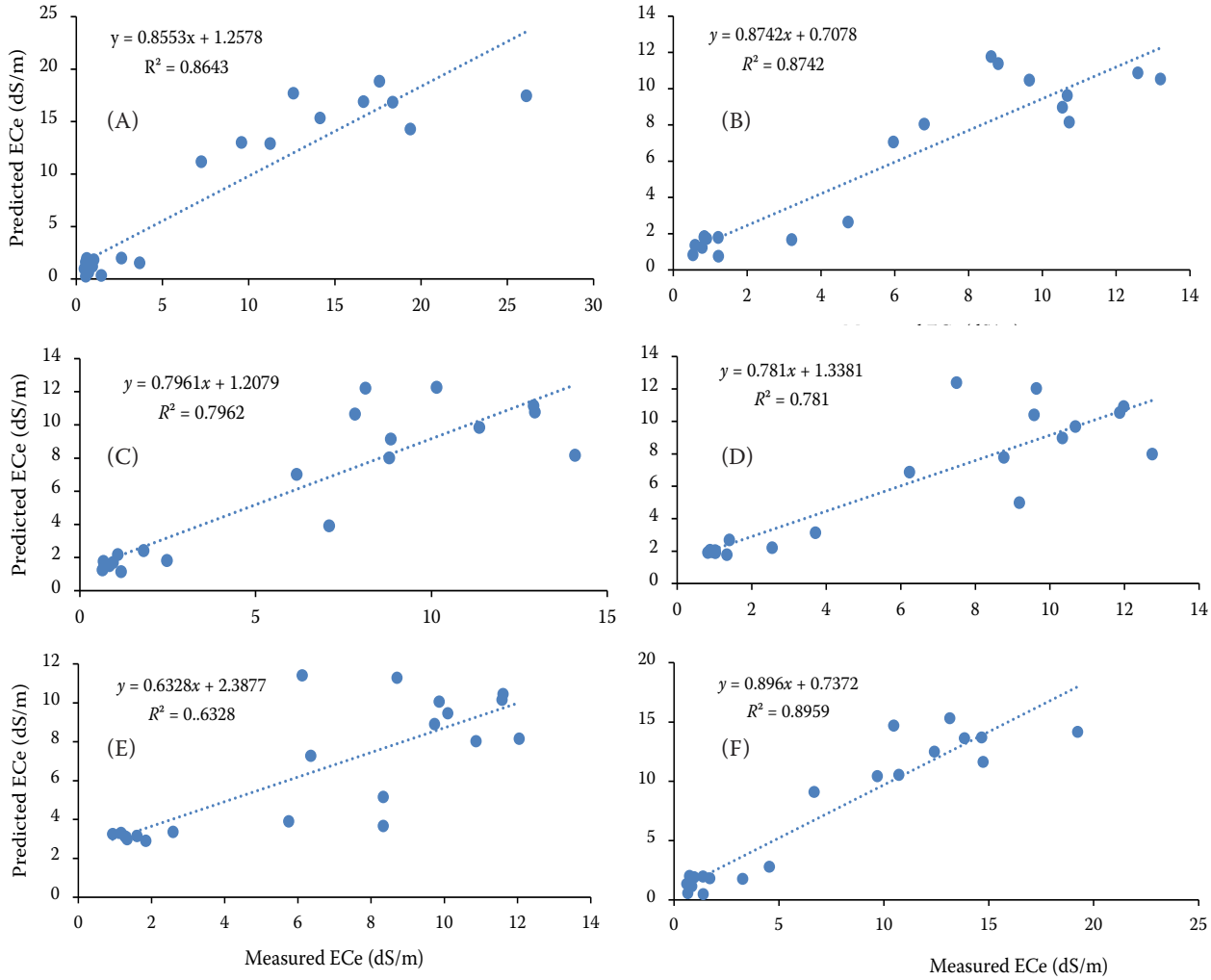

Figure 6. Scatter plots of the measured vs. predicted soil electrical conductivity (ECe): 0–20 cm (A), > 20–40 cm (B), > 40–60 cm (C), > 60–80 cm (D), > 80–100 cm (E) and 0–100 cm (F) using calibrated models

https://doi.org/10.17221/178/2020-SWR

Table 4. Semi-variogram parameters of the topsoil and average electrical conductivity and its validation

Location	Variables (dS/m)	Theoretical model	Nugget	Range	Sill	R^2	Residual error	SD
Ridges	average EC (0–100 cm)	exponential	1.13	702.01	8.65	0.92	1.05	1.94
	EC (0–20 cm)	exponential	2.83	813.83	1.46	0.79	1.03	2.53
Furrows	average EC (0–100 cm)	exponential	1.32	1 674.31	1.93	0.79	1.2	1.69
	EC (0–20 cm)	exponential	2.11	1 654.33	2.46	0.81	1.17	2.09

EC – electrical conductivity; SD – standard deviation

Table 5. Accuracy comparison for the two kriging methods

Interpolation method		Ridges			Furrows		
		R^2	RMSE	ME	R^2	RMSE	ME
Ordinary kriging	ECe (0–20 cm)	0.79	1.03	2.44	0.81	1.16	1.91
	average ECe	0.92	1.08	1.85	0.79	1.14	1.58
Universal kriging	ECe (0–20 cm)	0.79	1.03	2.44	0.81	1.16	1.91
	average ECe	0.92	1.08	1.85	0.79	1.14	1.58

ECe – soil electrical conductivity; RMSE – root mean squared error; ME – mean error

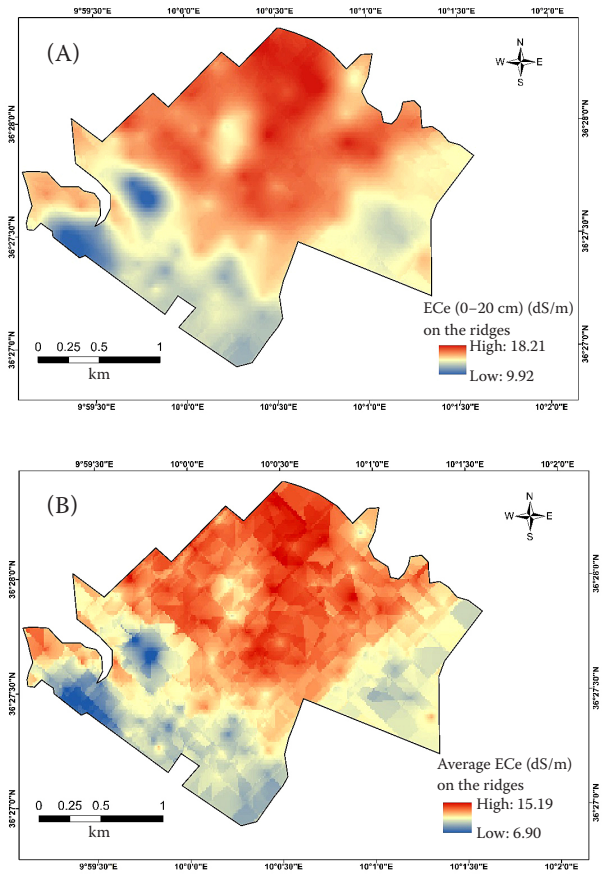

Figure 7. Spatial distribution of the soil electrical conductivity (ECe) on the ridges using ordinary kriging: ECe (0–20 cm) (A); average ECe (0–100 cm) (B)

furrows). This was due to inappropriate irrigation with brackish water during the spring. Besides, irrigation is practiced empirically without considering the real water requirements of the olive trees. Furthermore, the increased evapotranspiration level aggravates the severity of the soil salinity. Likewise, this can be explained by the surface geometry and the planting ridges where the drippers are located. In fact, the physicochemical properties of the soil give it the character of being heavy, not porous and not very permeable, which makes the salts' mobility slow and static and their lateral extension irregular and interrupted. The salts remain just on the ridges and their lateral migration towards the furrows is almost insignificant, which creates a net contrast over short distance. As reported in Table 5, the validation statistics (R-square, RMSE and ME values) are relatively the same for both interpolation methods (OK and UK). We also noted that OK and UK could achieve land cover mapping with a very good accuracy equally well.

Spectral index regression. For both images, we used stepwise regression considering the spectral indices as independent variables to obtain univariate and multivariate models which are displayed in Table 6.

For all the calibrated models, the R-square values range between 0.01 and 0.12, which indicates that the soil salinity indices adopted in this study are not good for predicting the ECe from remotely sensed

https://doi.org/10.17221/178/2020-SWR

Table 6. Univariate and multivariate regression models between the spectral indices and soil electrical conductivity of the top layer and average ECe (0–100 cm)

Acquisition date	Position	Regression models ($P < 0.01$)	R^2	RMSE	ME
April 30, 2019	furrows	ECe (0–20 cm) = 13.73 + 260.84 × BI – 396.72 × SI1 + 117 × SI3	0.121	2.24	5.02
		average ECe (0–100 cm) = 11.48 – 88.65 × SI1 + 58.03 × SI3	0.099	1.85	3.43
	ridges	ECe (0–20 cm) = 7.19 + 84.44 × ρOLI2	0.013	2.77	7.67
		average ECe (0–100 cm) = 6.17 + 65.41 × ρOLI2	0.012	2.19	4.82
May 16, 2019	furrows	ECe (0–20 cm) = 7.38 – 19.57 × ρOLI3	0.023	2.34	5.5
		average ECe (0–100 cm) = 6.91 – 16.67 × ρOLI3	0.025	1.92	3.68
	ridges	ECe (0–20 cm) = 12.15 + 6.35 × NDVI	0.01	2.77	7.7
		average ECe (0–100 cm) = 9.66 + 5.73 × NDVI	0.011	2.19	4.83

ECe – soil electrical conductivity; RMSE – root mean squared error; ME – mean error

data. The low correlation coefficients obtained for the spectral indices' multiple regression models, reflect a relatively narrow relationship between the soil salinity and the spectral indices for the case of clayey soils having accumulated salts in a linear, discontinuous and interrupted way. Besides, the images have a spatial resolution of 30 m which is smaller than the sampling interval adopted in this study which ranged between 50 and 100 m. Furthermore, the high vegetation cover in the olive orchard makes it that the remotely sensed data could provide information about the vegetation stress, but not directly about the soil salinity.

Previous studies (Wu et al. 2009; Ding & Yu 2014; Taghizadeh-Mehrjardi et al. 2014) have reported that combining the EMI system and remote sensing could provide information about the salt distribution fairly quickly, which was not our case. Nevertheless, it is convenient to remind the reader that the study area of Ding and Yu (2014) was a Delta Oasis between the Werigan and Kuqa River in the northern rim of Tarim Basin, Xinjiang, China, with a relatively meagre land cover, thus the remote sensed data are rich on information on the soil. Taghizadeh-Mehrjardi et al. (2014) underlined that most of their study area is bare land, therefore, a change in the soil conditions can be directly detected by remote sensing. Whereas, to improve the prediction of the ECe, Wu et al. (2009) established regression models based on a combination of the soil and land cover spectral indices. There are some plausible explanations behind our failure to predict the ECe based on spectral index regressions. Firstly, the surface geometry (i.e., presence of ridges and furrows) that causes a sudden change in the salt distribution (salts accumulated in a linear, discontinuous and interrupted manner). Secondly, the high vegetation cover and its reflectance influence the reflectance value from the multispectral image data. Thirdly, the spectral resolution of the multispectral data (30 × 30 m) is quite low, so the image data did not capture the soil salinity well. As

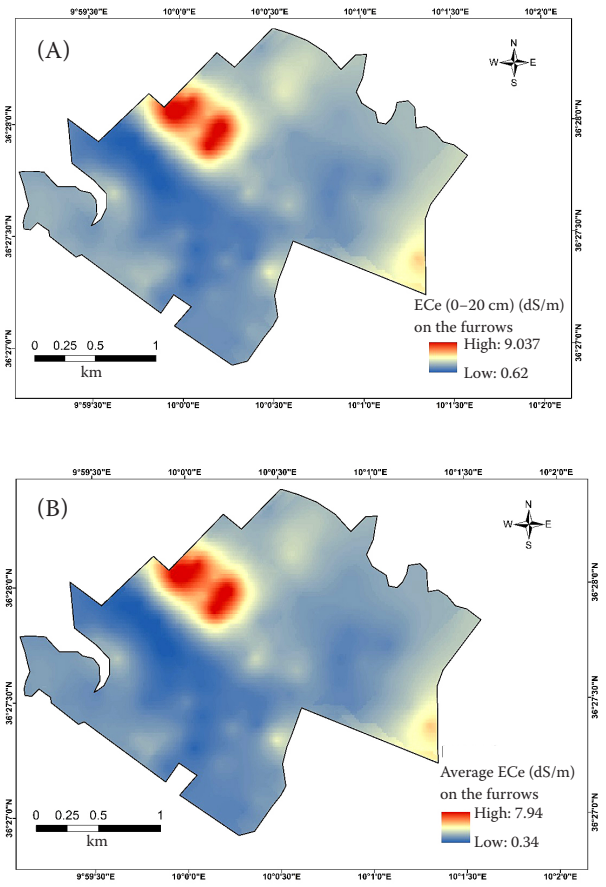

Figure 8. Spatial distribution of the soil electrical conductivity (ECe) on the furrows using ordinary kriging: ECe (0–20 cm) (A); average ECe (0–100 cm) (B)

https://doi.org/10.17221/178/2020-SWR

a result, the detection of the salts' spatial variability from the remotely sensed data is still challenging for an evergreen land cover. Metternicht and Zinck (2003) reported that lands with a canopy are problematic for soil salinity mapping by RS data.

CONCLUSION

Soil salinity mapping using the OK and UK method, based on EM38, at different depths within a VHD olive orchard landscaped in RF was accurately achieved and the spatial pattern of the salinity was finely described. Nevertheless, we failed in the soil salinity mapping based on the soil spectral indices. This is mainly explained by the fact that the olive tree canopy largely covers the land, which impeach to capture data on the soil from the remote sensed images. In future investigations, to improve the prediction performance of the spectral index model, plant indices, such as the leaf area index (LAI) and vegetation water content (VWC) derived from the remote sensing image data should be combined with soil the indices.

Notwithstanding, our results revealed a very strong localised salinisation that reaches intolerable values for the olive trees, especially on the top of the ridges (where the drippers are localised), in fact, such a result is related to the quality of the irrigation water, as saline water is the main source available in the semi-arid region. Such a kind of management can lead to soil degradation. Therefore, there is an urgent need to review this land management practice. It is recommended to combine the irrigation water supply from the Bir Mcherga Dam with salinity mitigation measures. Besides, improving the soil structure can lead to the creation of a more porous soil allowing for the faster mobility of the salts and their evacuation outside the root zone. This presumes a supply of organic matter and its burial under the drippers, this measurement must be accompanied by calcium intakes which may be beneficial to the soil structure and which alleviate the alkalisation process, gypsum spreading may be an appropriate solution for this calcium intake. Otherwise, looking for other irrigation water sources with better quality and a lower salinisation effect could be an option, though also, the use of deep groundwater or even groundwater would be a solution to avoid the strong salinisation recorded. Finally, it should be noted that the soils outside the perimeter have no aspect of salinisation, either primary or secondary, and that this process is essentially anthropogenic in this part of the Miliane watershed. This practice of irrigation combining salty water with fine textured soils is to be avoided in any hydro-agricultural project, especially in arid and semi-arid zones. This leads to the partial loss of soil resources and accentuation of the desertification process.

Acknowledgements. We would like to thank the two anonymous reviewers, their valuable comments and suggestions helped improve and clarify this manuscript.

REFERENCES

Abbas A., Khan S. (2007): Using remote sensing techniques for appraisal of irrigated soil salinity. In: Oxley L., Kulasiri D. (eds): MODSIM 2007 International Congress on Modelling and Simulation. Modelling and Simulation Society of Australia and New Zealand, Brighton, Dec 2007: 2632–2638.

Akramkhanov A., Brus D.J., Walvoort D.J.J. (2014): Geostatistical monitoring of soil salinity in Uzbekistan by repeated EMI surveys. Geoderma, 213, 600–607.

Amezketa (2007): Soil salinity assessment using directed soil sampling from a geophysical survey with electromagnetic technology: a case study. Spanish Journal of Agricultural Research, 5: 91–101.

Bannari A., Guedon A.M., El-Harti A., Cherkaoui F.Z., El-Ghmari A. (2008): Characterization of slightly and moderately saline and sodic soils in irrigated agricultural land using simulated data of advanced land imaging (EO-1) sensor. Communications in Soil Science and Plant Analysis, 39: 2795–2811.

Boudabous K., Ben Aissa N., Trifa Y., Sahli A., Slim Amara H. (2016): Soil microorganisms alleviates the negative effect of salinity on morpho-physiological characteristics during growth stages of durum wheat genotypes. Journal of New Sciences, 28: 1622–1630.

Bouksila F., Persson M., Berndtsson R., Bahri A. (2010): Estimating soil salinity over a shallow saline water table in semiarid Tunisia. The Open Hydrology Journal, 4: 91–101.

Chavez P.S.J. (1996): Image-based atmospheric corrections – revisited and improved. Photogrammetric Engineering and Remote Sensing, 62: 1025–1036.

CRUESI (1970): Research and Training in Saltwater Irrigation, 1963–1969. Technical Report-Tunisia, Paris, PNUD-UNESCO. (in French)

Deering D., Rouse J. (1975): Measuring 'forage production' of grazing units from Landsat MSS data. In: 10th Int. Symp. Remote Sensing of Environment, ERIM, Ann Arbor, 1975: 1169–1178.

https://doi.org/10.17221/178/2020-SWR

Ding J., Yu D. (2014): Monitoring and evaluating spatial variability of soil salinity in dry and wet seasons in the Werigan-Kuqa Oasis, China, using remote sensing and electromagnetic induction instruments. Geoderma, 235–236: 316–322.

Douaoui A.E.K., Nicolas H., Walter C. (2006): Detecting salinity hazards within a semiarid context by means of combining soil and remote-sensing data, Geoderma, 134: 217–230.

Farifteh J., Van der Meer F., Atzberger C., Carranza E.J.M. (2007): Quantitative analysis of salt-affected soil reflectance spectra: A comparison of two adaptive methods (PLSR and ANN). Remote Sensing of Environment, 110: 59–78.

Filippi L (2017): Olive Oil, Tunisia's "Green Gold". Information Bulletin of the National Office of the Oil. Available at http://www.bulletin.onh.com.tn/actualites-detail.php?id=179. (in French)

Hachicha M (2016): Gestion des ressources en sols sous irrigation avec les eaux salées. National Research Institute in Rural Engineering, Water and Forestry, University of Carthage.

Hillel D., Vlek P. (2005): The sustainability of irrigation. Advances in Agronomy, 87: 55–84.

Kahlaoui B., Hachicha M., Rejeb S., Rejeb M.N., Hanchi B., Misle E. (2011): Effects of saline water on tomato under subsurface drip irrigation: nutritional and foliar aspects. Journal of Soil Science and Plant Nutrition, 11: 69 – 86.

Khan N.M., Rastoskuev V., Sato Y., Shiozawa S. (2005): Assessment of hydrosaline land degradation by using a simple approach of remote sensing indicators. Agricultural Water Management, 77: 96–109.

Knotters M., Heuvelink G.B.M., Hoogland T., Walvoort D.J.J. (2010): A Disposition of Interpolation Techniques. Wageningen, Statutory Research Tasks Unit for Nature and the Environment, WOt-werkdocument 190.

Larbi A.S. Vazquez H., El-Jendoubi M., Msallem J., Abadıa A., Morales F. (2015): Canopy light heterogeneity drives leaf anatomical, eco-physiological, and photosynthetic changes in olive trees grown in a high-density plantation. Photosynthesis Research, 123: 141–155.

Larbi A., Msallem M., Mestaoui S., Sai M.B., El Gharous M., Boulal H. (2016): Fertilization practices in Tunisian high-density olive planting systems. Better Crops, 100: 9–11.

Li X.-M., Yang J.-S., Liu M.-X., Liu G.-M., Yu M. (2012): Spatio-temporal changes of soil salinity in arid areas of south Xinjiang using electromagnetic induction. Journal of Integrative Agriculture,11: 1365–1376.

Liu G., Li J., Zhang X., Wang X., Lv Z., Yang J., Shao H., Yu S. (2016): GIS-mapping spatial distribution of soil salinity for eco-restoring the Yellow River Delta in combination with electromagnetic Induction. Ecological Engineering, 94: 306–314.

Liu G.M., Yang J.S., Ju M.S., Nie J. (2003): Technology of chorometry using electromagnetic induction and its application in agriculture. Soils, 35: 27–29.

Masmoudi C.C., Msallem M., Larbi A., Sai B., Siala S., Kchaou M. (2017): Establishment and Conduct of an Intensive Plantation of Olive Trees. Tunis, Institution de la Recherche et de l'Enseignement Supérieurs Agricoles Institut de l'Olivier -Station du Nord. (in French)

Mesić Kiš I. (2016): Comparison of ordinary and universal kriging interpolation techniques on a depth variable (a case of linear spatial trend), case study of the Šandrovac Field. Rudarsko Geolosko Naftni Zbornik. The Mining-Geology-Petroleum Engineering Bulletin UDC: 528. 9:912.

Metternicht G.I., Zinck J.A. (2003): Remote sensing of soil salinity: Potentials and constraints. Remote Sensing of Environment, 85: 1–20.

Michot D., Walter C., Adam I., Guéro Y. (2013): Digital assessment of soil-salinity dynamics after a major flood in the Niger River valley. Geoderma, 208: 193–204.

Oliver M., Webster R. (2014): A tutorial guide to geostatistics: Computing and modelling variograms and kriging. Catena, 113: 56–69.

Ouji A., El-Bok S., Mouelhi M., Ben Younes M., Kharrat M. (2015): Effect of salinity stress on germination of five Tunisian lentil (*Lens culinaris* L.) genotypes. European Scientific Journal, 11: 63–75.

Radinovsky L. (2019): Worldwide Olive Oil Production Estimates Compared. Available at http://www.greekliquidgold.com/index.php/en/news/351-2018-19-worldwide-olive-oilproduction-estimates-compared (accessed March 3, 2019).

Richards L.A. (1954): Diagnosis and Improvement of Saline and Alkali Soils. Handbook No. 60, Washington, U.S. Salinity Laboratory Staff.

Shrestha R.P. (2006): Relating soil electrical conductivity to remote sensing and other soil properties for assessing soil salinity in northeast Thailand. Land Degradation and Development, 17: 677–689.

Taghizadeh-Mehrjardi R., Minasny B., Sarmadian F., Malone B.P. (2014): Digital mapping of soil salinity in Ardakan region, central Iran. Geoderma, 213: 15–28.

Tucker C.J. (1979): Red and photographic infrared linear combinations for monitoring vegetation. Remote Sensing of Environment, 8: 127–150.

Webster R., Oliver M.A. (2007): Geostatistics for Environmental Scientists. 2nd Ed. Chichister, John Wiley and Sons.

Wu Y.K., Yang J.S., Li X.M. (2009): Study on spatial variability of soil salinity based on spectral indices and

https://doi.org/10.17221/178/2020-SWR

EM38 readings. Spectroscopy and Spectral Analysis, 29: 1023–1027.

Yao R.J., Yang J.S., Zou P., Liu G.M., Yu S.P. (2008): Quantitative evaluation of the field soil salinity and its spatial distribution based on electromagnetic induction instruments. Scientia Agricultura Sinica, 41: 460–469.

Yao R.J., Yang J.S., Wu D.H., Xie W.P., Cui S.Y., Wang X.P., Yu S.P., Zhang X. (2015): Determining soil salinity and plant biomass response for a farmed cropland using the electromagnetic induction method. Computers and Electronics in Agriculture, 19: 241–253.

Zhang T.J., Yang J.S., Liu G.M., Yao R.J. (2009): Interpretation of salinity characteristics of normal profile in estuarine region by using electromagnetic induction. Transactions of the Chinese Society of Agricultural Engineering, 25: 109–113.

Received: December 20, 2020
Accepted: May 17, 2021
Published online: October 22, 2021